

## ARTICLE OPEN



# A new route to fabricate flexible, breathable composites with advanced thermal management capability for wearable electronics

Huibao Chen<sup>1,2,13</sup>, Yafei Ding<sup>3,13</sup>, Guimei Zhu<sup>4</sup>, Yu Liu<sup>2</sup>, Qun Fang<sup>5</sup>, Xue Bai<sup>6</sup>, Yan Zhao<sup>7</sup>, Xin Li<sup>1</sup>, Xingyi Huang<sup>8</sup>, Tong-Yi Zhang<sup>9</sup>, Baowen Li<sup>3,10,11</sup> and Bin Sun<sup>1,2,12</sup>

Wearable electronics with miniaturization and high-power density call for devices with advanced thermal management capabilities, outstanding flexibility, and excellent permeability. However, it is difficult to achieve these goals simultaneously due to the conflict between high thermal conductivity and permeability and flexibility. Here, we report an approach to fabricate flexible, breathable composites with advanced thermal management capability by coating the boron nitride nanosheets (BNNs) layer with high thermal conductivity on the grids of patterned electrospun thermoplastic polyurethane (TPU) fibrous mats. The composite exhibited a significant enhancement of thermal conductivity and preserved instinctive breathability simultaneously. When the composite was integrated into flexible devices, its saturating operating temperature dropped significantly compared to that of pure Ecoflex packaging. Moreover, the surface temperature fluctuation was less than 0.5 °C during more than 2000 cycles bending-releasing process. Finally, a prototype to fabricate wearable electronics with advanced thermal management capability was proposed.

*npj Flexible Electronics* (2023)7:24; <https://doi.org/10.1038/s41528-023-00257-0>

## INTRODUCTION

Flexible/stretchable devices have gained increasing attention due to their potential applications in various fields such as sensors<sup>1–5</sup>, light-emitting diodes (LEDs)<sup>6–8</sup>, energy harvest and storage devices<sup>9–13</sup>, photodetectors<sup>14,15</sup>, human-machine interfaces<sup>16–18</sup>. Particularly, with the booming of the Internet of Things (IoT) and artificial intelligence (AI), wearable electronics have been gradually penetrating into our daily lives because of their potential applications in human health monitoring, human senses detection, and movement assistance<sup>18–20</sup>. To achieve ideal functionality under mechanical deformation of such devices, electrical components have to be integrated with polymers, by either directly embedding nanomaterials into polymer matrixes; and/or transferring active materials onto the surface of elastic substrates<sup>21</sup>. In addition to the outstanding electrical and mechanical properties, other important features such as excellent permeability of air, sweat vapor, and even liquid, are highly desired for an ideal wearable electronic device, to avoid serious discomfort and even skin irritation during long-term wearing<sup>22–24</sup>.

Electrospinning is a versatile technique for fabricating nano/micro fibers with a variety of outstanding properties, such as large surface area, high length-to-diameter ratio, flexible surface functionality, and tunable surface morphologies. The porous electrospun fibrous membrane is proved to act as substrate and/or matrix for flexible devices with good permeability<sup>1,23,25,26</sup>.

Due to the porous architecture, electrospun fibrous mats usually have low thermal conductivity, and are used as a thermal insulator. Among numerous polymers that can be electrospun, thermoplastic polyurethane (TPU) has drawn researchers' attention due to its biocompatibility, hydrophobicity, and high resistance to tearing and oxidation<sup>1,26,27</sup>. Specially, the high elasticity, flexibility, and toughness of TPU make it a valuable substrate and packaging for flexible/stretchable devices. We have designed a stretchable strain sensor based on graphene nanoribbons<sup>1</sup>, where electrospun TPU porous fibrous membrane with a suppressed thermal conductivity and good breathability is introduced as thermal insulating layers. Nevertheless, the lateral directional breathability of the sample cannot meet the real needs of modern wearable electronics.

On the other hand, with the rapid growth of next-generation electronic devices, the dense integration, miniaturization, and large power density of such devices leads to a severe accumulation of waste heat in their composition, thus advanced thermal management has become critical to ensure safe operation<sup>28–33</sup>. In general, crystalline materials such as metal, carbon-based materials (graphene, carbon nanotubes (CNTs)), and ceramics have high thermal conductivity ( $k$ )<sup>34</sup>. However, the rigid nature hinders the further application of flexible electronics. Polymers with preponderance such as easy processing, lightweight, high deformability, and low manufacturing cost, have been widely adopted for electronic devices and integrated circuit packaging,

<sup>1</sup>College of Physics, Qingdao University, Qingdao 266071, PR China. <sup>2</sup>College of Electronics and Information, Qingdao University, Qingdao 266071, PR China. <sup>3</sup>Department of Materials Science and Engineering, Southern University of Science and Technology, Shenzhen 518055, PR China. <sup>4</sup>School of Microelectronics, Southern University of Science and Technology, Shenzhen 518055, PR China. <sup>5</sup>School of Physical Education, Qingdao University, Qingdao 266071, PR China. <sup>6</sup>Shenzhen Institute of Advanced Electronic Materials, Shenzhen Institute of Advanced Technology, Chinese Academy of Sciences, Shenzhen 518055, PR China. <sup>7</sup>College of Textile and Clothing Engineering, Soochow University, Suzhou 215123, PR China. <sup>8</sup>Department of Polymer Science and Engineering, Shanghai Key Laboratory of Electrical Insulation and Thermal Aging, Shanghai Jiao Tong University, Shanghai 200240, PR China. <sup>9</sup>Materials Genome Institute, Shanghai University, 200444 Shanghai, PR China. <sup>10</sup>Department of Physics, and Shenzhen International Quantum Academy, Southern University of Science and Technology, Shenzhen 518055, PR China. <sup>11</sup>Paul M Rady Department of Mechanical Engineering, Department of Physics, University of Colorado, Boulder, CO 80305-0427, USA. <sup>12</sup>Weihai Innovation Research Institute of Qingdao University, Weihai 264200, PR China. <sup>13</sup>These authors contributed equally: Huibao Chen, Yafei Ding. ✉email: zhugm@sustech.edu.cn; xue.bai@siat.ac.cn; yanzhao@suda.edu.cn; qdusun@qdu.edu.cn

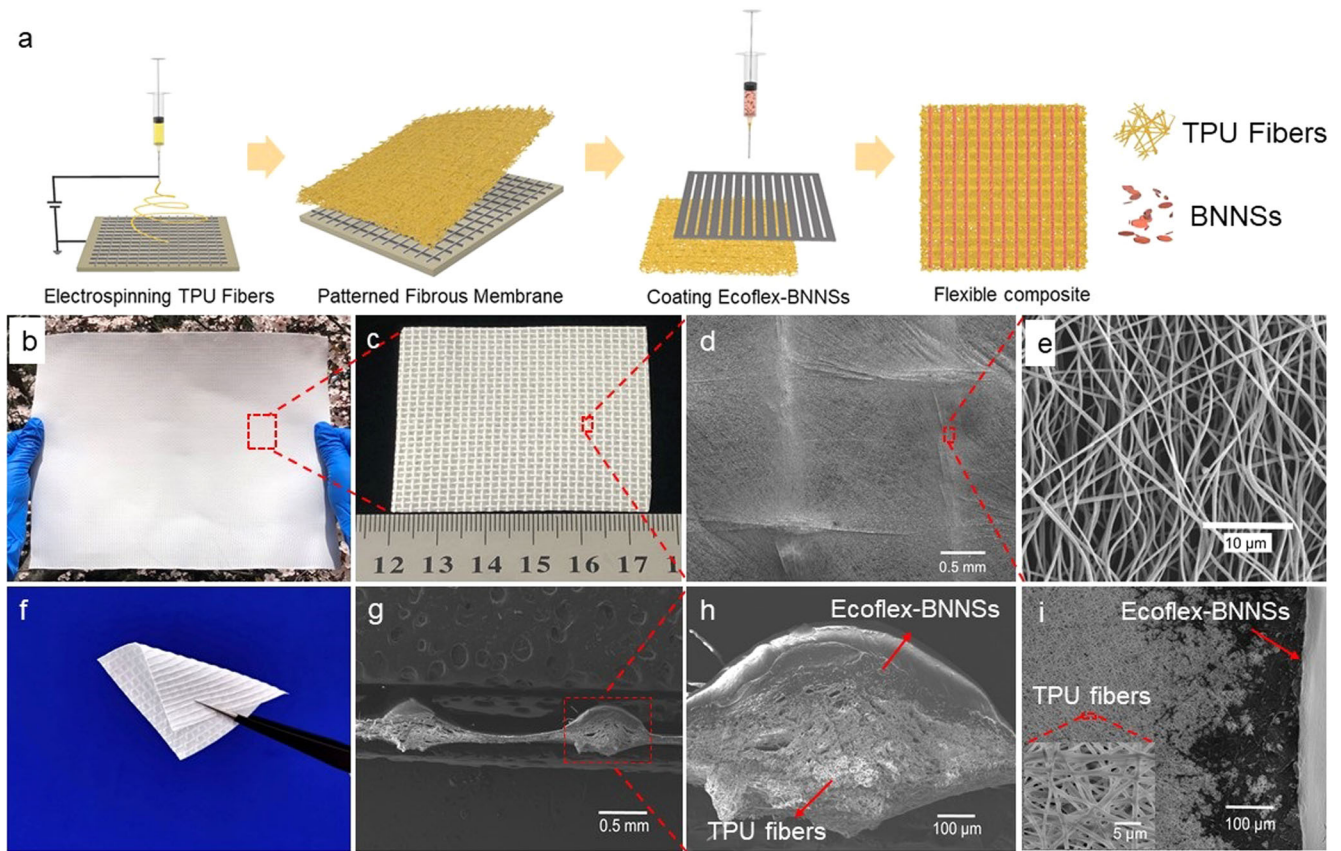


**Fig. 1 Basic characterization.** **a** The fabrication process of the composite. **b, c** Photographs of the patterned electrospun TPU fibrous membrane, which was analogous to the metal collector. **d, e** SEM images of the patterned electrospun TPU fibers. Relative alignment of the fibers can be found on the warps and wefts. **f** Photograph of the sample covered with Ecoflex-BNNSs layers on the fibrous grids. **g, h** Cross-sectional SEM images of the fibrous grids covered with Ecoflex-BNNSs layers. **i** Even after depositing the Ecoflex-BNNSs layer, the pores among the warps and wefts remained the breathability of the composite (Insert is the enlarged SEM image of the fibers among the grids after coating Ecoflex-BNNSs layer).

but they always have low intrinsic thermal conductivity (less than  $\sim 0.5 \text{ W}\cdot\text{m}^{-1}\cdot\text{K}^{-1}$ ), which limits applications in the field of thermal dissipation. To overcome this barrier, nanocomposites composed of an insulating polymer matrix and highly thermally conductive inorganic fillers are usually adopted, by integrating the mechanical stability of polymers and the high thermal conductivity of inorganic fillers<sup>34,35</sup>.

To achieve high heat dissipation, one needs to have high thermal diffusivity,  $a = k/(\rho\cdot c_p)$ , where  $\rho$ ,  $c_p$ , and  $k$  denote the mass density, specific heat, and thermal conductivity of the composite, respectively. On the other hand, thermal conductivity depends on elasticity<sup>36</sup>, according to

$$k \approx \frac{C_V l}{3} \sqrt{\frac{E}{\rho}} \quad (1)$$

Therefore, the thermal diffusivity  $a$  is proportional to  $\sqrt{E}$  and inverse proportional to  $\rho^{3/2}$ . Obviously, a large elasticity modulus is favorable to heat diffusion. However, a large elasticity modulus is against flexibility. Therefore, making a wearable electronic device with good permeability, flexibility, and high thermal conductivity are very challenging and appear to be a “mission impossible”.

In this work, we achieve this “impossible mission” by fabricating a composite integrated with advanced thermal management capability, outstanding flexibility, and excellent permeability. This composite was fabricated based on patterned electrospun TPU fibrous mats, followed by coating Ecoflex-BNNSs layers along the

grids of the patterned architectures. BNNS is selected because it has an ultrahigh thermal conductivity ( $\sim 1700\text{--}2000 \text{ W}\cdot\text{m}^{-1}\cdot\text{K}^{-1}$ ), and a high-aspect ratio two-dimensional (2D) morphology. Moreover, it is an electrical insulator that can prevent it from the possible signal shielding and short circuit problem when used for the thermal management and packaging for the modern electrical equipment and electronic devices<sup>37</sup>. As a result, the composite demonstrated a 4442% enhancement of the thermal conductivity compared to the pure patterned fibrous structure while maintaining the inherent breathability. After integrating it into flexible devices, the saturating operating temperature of the sample with 25 wt% BNNSs demonstrated a drastic dropping than that with pure Ecoflex packaging. Even during more than 2000 cycles of continuously bending-releasing process, the surface temperature fluctuated within a small range of less than  $0.5 \text{ }^\circ\text{C}$ , which was only one-sixth of that with pure Ecoflex packaging. At last, a prototype to prepare wearable electronics with desired architecture and advanced thermal management capability has been proposed. Our results should be able to provide a feasible route for the fabrication of next-generation of wearable devices.

## RESULTS

### Fabrication and structure of the composite film

The fabrication process of the composite is shown in Fig. 1a. The patterned electrospun TPU fibers were obtained using a metal grid collector, and the as-exfoliated BNNSs were deposited along the grids of the patterned fibrous membrane. During traditional

electrospinning, the precursor solution firstly emerged from a spinneret to form a small droplet, and charged under the electric field. Then the charged solution was extruded from the cone as jets. Undergoing vigorous whipping and/or splitting motions due to fluid instability, electrically driven bending instability, and the volatilization of the solvent, the jets became continuous electrospun fibers and deposited on the collector as 2D nonwoven fibrous membrane. However, the random orientation of the as-spun fibers limit their further applications, and morphology-controlled micro-/nanofibrous architectures have been a crucial issue<sup>38</sup>. Among the structure-controlled electrospun products, patterned fibrous architecture can be generated using metal grids as collector. Due to the redistribution of the static electric field during electrospinning<sup>39</sup>, a patterned architecture similar to the metal collector can be achieved. Figure 1b–e demonstrates the morphology and structure of the as-spun TPU fibrous mats in this experiment. It can be seen that the fibrous web can be assembled on a large scale according to the size of the metal grid collector (Fig. 1b). After peeling off from the collector, the electrospun membrane demonstrate a regular morphology with the warps and wefts, analogous to the collector (Fig. 1c, d and Supplementary Fig. 1). In the areas among the warps and wefts, less fibers were deposited, resulting in the large porosity, as shown in Fig. 1d, while in the areas of the warps and wefts, relatively aligned fibrous arrays can be observed, as shown in Fig. 1d, e, which hence rendered better mechanical property along the axis direction compared to the nonwoven counterpart (Supplementary Fig. 2).

The BNNSs were exfoliated from commercial bulk *h*-BN powders according to our previous works<sup>1,40,41</sup>, revealing a typical 2D structure with an extremely high aspect ratio, as shown in Supplementary Fig. 3. The as-exfoliated BNNSs mixed with Ecoflex were coated onto the grids of the patterned TPU fibrous membrane with the aid of a metal mask. In this case, the reason for introducing Ecoflex was ascribed to the outstanding elasticity, non-crystallization, and the almost low thermal conductivity ( $0.16 \text{ W m}^{-1} \text{ K}^{-1}$ ) compared to TPU<sup>42</sup>. Most importantly, the ingredients of Ecoflex were incapable of damaging the fibers and the fibrous structure. Namely, Ecoflex layer will not cause an obviously negative impact on the properties of TPU electrospun film. From Fig. 1f, one can see that after coating Ecoflex-BNNSs, the composite film still retained excellent flexibility. And even with the BNNSs loading of 25 wt%, it can be stretched to more than 600%, a little higher than that without Ecoflex-BNNSs (Supplementary Fig. 2b). The reason can be attributed to the better mechanical compliance of Ecoflex than that of TPU, and the good adhesion between Ecoflex-BNNSs and TPU fibers, illustrating the outstanding mechanical property of the composite. The combination of Ecoflex-BNNSs and TPU fibers was validated by the SEM images of the sample. As shown in Fig. 1g, Ecoflex-BNNSs were well coated on the grids of the fibrous structure, while the region between the grids were porous fibers. From the enlarged cross-sectional SEM image (Fig. 1h), one can see that Ecoflex-BNNSs were bonded with electrospun TPU fibers, and the interfaces between Ecoflex-BNNSs layer and the fibrous membrane were blurry, rendering a wonderful integration of the components. Even after more than 1000 cycles of bending and stretching (100%), no obvious separation was observed, as shown in Supplementary Fig. 4. This good adhesion between Ecoflex-BNNSs and TPU fibers, as well as the stability, was also contributing to the exceptional elasticity of the sample.

### Breathability of the composite film

As is known, breathability or gas permeability is a crucial factor for wearable electronics because of the safety requirements. Devices with poor gas permeability can cause discomfort and

irritation of human skin<sup>1,24</sup>. The unique patterned fibrous structure ensure the composite film has a large porosity in the areas among the grids, leading to good permeability. Even after depositing BNNSs, the fibrous pores in these fields were almost unchanged (Fig. 1i). Thus the air flow can effortlessly penetrate the fibrous mats vertically, retaining the good breathability of the composite compared to the pure fibrous membrane (Fig. 2a). After tested, the air permeability of the patterned fibrous membrane before and after coating Ecoflex-BNNSs layer changed from  $27.54 \text{ mm s}^{-1}$  to  $21.43 \text{ mm s}^{-1}$  (Fig. 2b). This was because the coating of Ecoflex-BNNSs strips concealed some originally pored region adjacent to the fibrous grids, however, numerous unaffected pores preserved the superior gas permeability, which was confirmed by the SEM images in Fig. 1i. Next, the composite film with Ecoflex-BNNSs layer was attached to an opening bottle containing DI water, and the permeability of water vapor can be evaluated by measuring the weight loss of water. As a comparison, a variety of conditions were respectively estimated, in which bottles were covered with plastic wrap, pure patterned TPU fibrous membrane, and uncovered. In this experiment, the samples were placed in a thermostatic chamber at room temperature and the humidity was 30% RH (Relative Humidity). It was found that the weight of the bottle with composite film with Ecoflex-BNNSs decreased at the approximate rate as the bottle with pure patterned fibrous membrane, and the bottle uncovered. On the contrary, the weight of the bottle covered with plastic wrap barely decreased after 240 h, as shown in Fig. 2c. This result evidently demonstrates the high degree of air/gas permeability of the as-prepared composite film, and strongly validated the possibility for wearable electronic devices.

### Thermal conductivity

TPU, as well as its fibers, is widely used in flexible/stretchable electronics<sup>43,44</sup>. However, the thermal properties of electrospun TPU fibers remain unknown, although electrospinning is reported to significantly improve the thermal conductivity of other polymers (e.g., polyethylene (PE)<sup>45,46</sup> and Nylon<sup>47</sup>) by generating ultrathin fibers, accompanied with an increased tensile modulus because of the chain alignment of fibers. Although the increased tensile modulus leads to unsuitability for the application of flexible electronic<sup>48–50</sup>.

Herein, the thermal conductivity of individual TPU fiber was measured by the thermal bridge method<sup>51,52</sup>. A suspended micron device contains two silicon nitride (SiN<sub>x</sub>) membranes and twelve beams, which are covered with platinum resistance thermometer (PRT) coils that served as heater and sensor in the measurement since the platinum resistance changes with temperature. To evaluate the thermal conductivity of the pristine individual TPU fiber, this suspended micron device was placed on the collector to receive the electrospun TPU fibers. By adjusting the electrospinning time, there is a probability that one or more suspended fibers will cross the two membranes, as shown in Fig. 3a. Only one fiber sample was selected while the other fibers were removed by a nanomanipulator or cut through by the Focused Ion Beam (FIB). The whole suspended device was placed in a cryostat with a vacuum level of around  $1 \times 10^{-6}$  mbar to reduce the effects of heat convection. A direct current (*I*) was applied on one PRT to generate a Joule heat  $Q = I^2 R_h$  and raise the temperature of one membrane, where  $R_h$  is the total heating resistance including the PRT of heater membrane and beams. Part of the Joule heat was conducted through the suspended fiber to the other membrane. The temperature changes at the two PRT were measured through the platinum resistance changes by a small alternating current.

The thermal conductance of the sample ( $G_s$ ) can be calculated as  $G_s = \frac{\Delta T_s Q}{(\Delta T_h - \Delta T_s) l}$ , where  $\Delta T_h$  and  $\Delta T_s$  are the temperature rise at the heater and sensor, and  $Q$  is the Joule heat dissipation in the heater

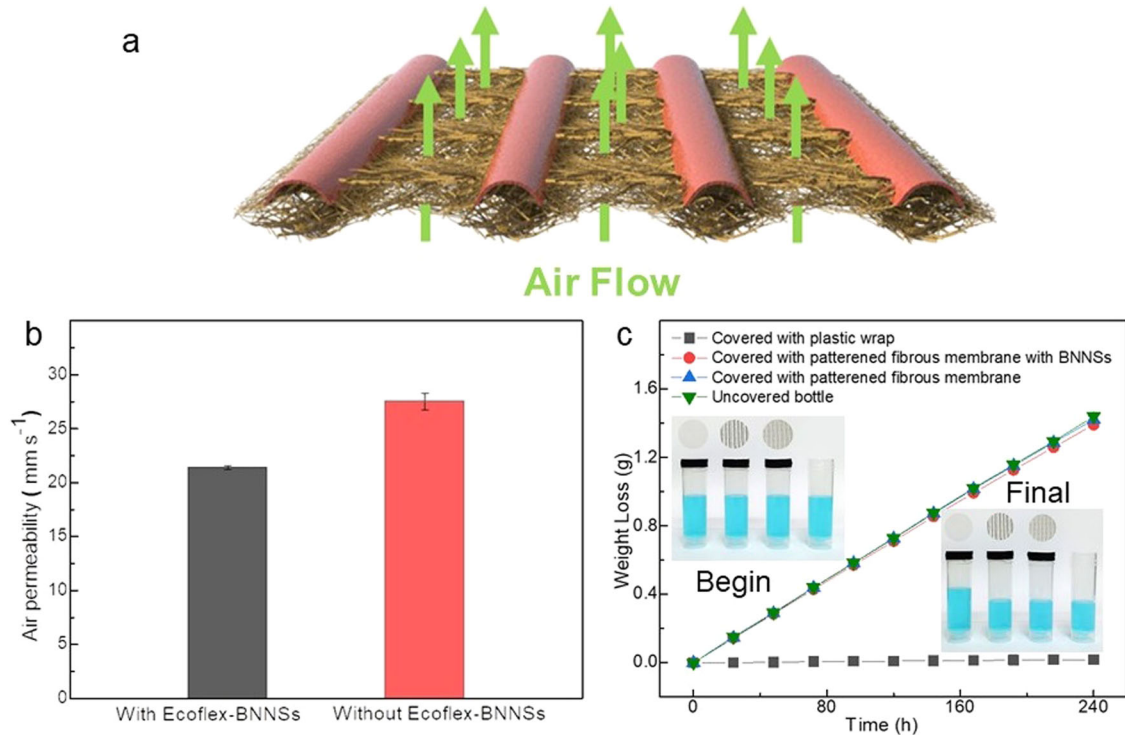


**Fig. 2 Breathability of the composite film.** **a** Schematic diagram of the permeability of the composite based on patterned fibrous structure. **b** Comparison of the air permeability of the patterned fibrous membrane before and after coating with Ecoflex-BNNSs layer. **c** Comparison of the water vapor permeability of the samples by covering water-containing opening bottles. The composite film with Ecoflex-BNNSs layer showed the approximate rate as the bottle with pure patterned fibrous membrane, and the bottle uncovered. On the contrary, the weight of the bottle covered with plastic wrap barely decreased after a long time running (Insert from left to right are the water contents of the bottles which were covered with plastic wrap, patterned TPU fibrous membrane with Ecoflex-BNNSs layer, pure patterned TPU fibrous membrane, and uncovered, respectively).

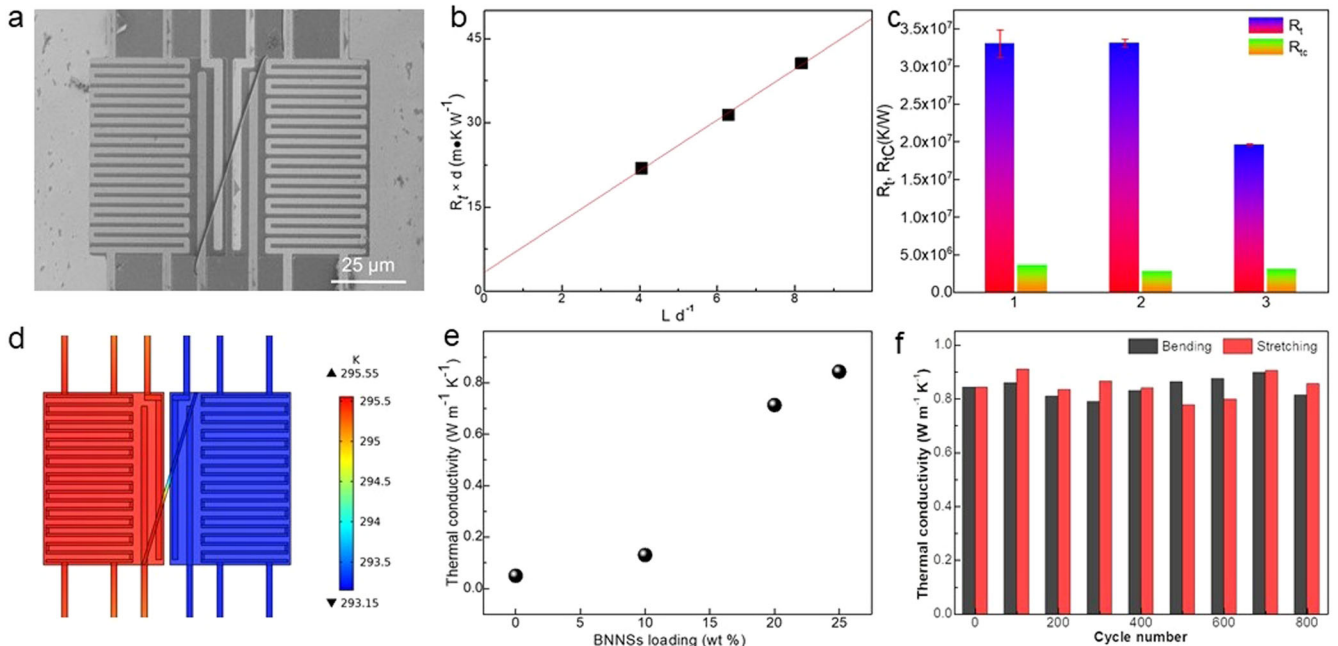


**Fig. 3 Thermal properties of the samples.** **a** SEM image of a single TPU fiber on the suspended device for thermal bridge measurement. **b** The linear fit of  $R_t \times d$  product as a function of  $L/d$  ratio. **c** The measured thermal resistance ( $R_t$ ) and thermal contact resistance ( $R_{t,c}$ ) vs. sample. **d** COMSOL Multiphysics simulated temperature distribution of Sample 1 on the thermal bridge. **e** Thermal conductivity of the samples with different contents of BNNSs, which were tested using Hot Disk TPS 2500S. **f** Thermal conductivity of the nanocomposite with 25 wt% BNNSs under multiple bending and stretching cycles.

**Table 1.** Measured thermal conductivity of samples.

Sample number	$d$ ( $\mu\text{m}$ )	$L$ ( $\mu\text{m}$ )	$k$ ( $\text{W m}^{-1}\text{K}^{-1}$ )
S1	$0.95 \pm 0.07$	$5.99 \pm 0.02$	$0.28$ ( $0.286 \pm 0.018$ )
S2	$1.23 \pm 0.03$	$10.04 \pm 0.01$	$0.28$ ( $0.280 \pm 0.005$ )
S3	$1.12 \pm 0.09$	$4.52 \pm 0.02$	$0.28$ ( $0.278 \pm 0.002$ )

TPU and one of the Pt beam<sup>53,54</sup>. The measured thermal resistance ( $R_t = G_s^{-1}$ ) includes the intrinsic thermal resistance of the suspended sample ( $R_{ts}$ ) and the thermal contact resistance between the fiber and the membranes ( $R_{tc}$ ). In order to remove the influence of thermal contact resistance, the room temperature thermal resistances of three samples with similar diameters ( $d$ ) but different suspended lengths ( $L$ ) have been measured. Since the contact resistance is inversely proportional to the contact width<sup>55</sup>, the  $R_t \times d$  product was plotted as a function of  $L/d$ , as shown in Fig. 3b. When  $L = 0$ ,  $R_t \times d = R_{tc} \times d$ , the thermal contact resistance  $R_{tc}$  of three samples can be calculated as  $3.55 \times 10^6$ ,  $2.76 \times 10^6$ ,  $3.03 \times 10^6 \text{ K W}^{-1}$ , respectively, which are consistent with previous reported thermal contact resistance of other samples in thermal bridge method<sup>56</sup>, indicating the thermal contact resistance within a reasonable range. Figure 3c shows the measured thermal resistance ( $R_t$ ) and thermal contact resistance ( $R_{tc}$ ). By removing the effect from contact resistance, the intrinsic thermal conductivity of the suspended TPU fiber can be calculated by  $k = \frac{4L}{\pi d^2 R_{ts}}$ , as shown in Table 1.

To verify the validity of the measured thermal conductivity of individual TPU fiber, a finite element simulation was conducted by COMSOL Multiphysics, as shown in Fig. 3d. The thermal bridge model settings were consistent with the real device, and the physical property parameters used in the simulation can be found in the previous study<sup>53,57</sup>. The simulated temperatures at the suspended edges of the sample fiber were close to that of TPU on each membrane, and their temperature difference is less than 0.01 K. Therefore, the temperature drop between the suspended two sample edges can be calculated as the temperature difference between the heater and the sensor TPU. Besides, the average raised temperature ratio of the two membranes in the simulation shows a general consistency with the measured temperature, which reveals that the value of the measured thermal conductivity of individual TPU fiber is reasonable.

The measured thermal conductivity of individual TPU fiber was around  $0.28 \text{ W m}^{-1}\text{K}^{-1}$ , which was close to that of bulk TPU. Although the stretching process during electrospinning has been reported to boost ordered molecular chains in polymers, showing a dramatic thermal conductivity increase as the electrospun fiber diameter is less than  $150 \text{ nm}$ <sup>47,53</sup>. In our experiment, the diameter of the electrospun TPU fibers is around  $1 \mu\text{m}$ , which is far from reaching an effective stretching process to increase molecular chain alignment in TPU<sup>49</sup>. Thus, the electrospun fibers maintained low elasticity modulus (Supplementary Fig. 2), a desirable feature for wearable flexible electronics. And the enhancement of the samples was mainly attributed to the addition of highly thermally conductive materials (BNNs).

For coating highly thermally conductive layers, the as-exfoliated BNNs were mixed with Ecoflex with an increasing loading of 10 wt%, 20 wt%, and 25 wt%, respectively. And the composite layers have the thickness of about 0.3 mm. When the content of BNNs was more than 25 wt%, it became viscous and lack of liquidity. As a proof of concept, after depositing Ecoflex-BNNs layer on the patterned TPU fibrous grids, the thermal conductivity of the samples have been significantly improved. As shown in Fig. 3e, the thermal conductivity of the composite with 25 wt% BNNs reached  $0.844 \text{ W m}^{-1}\text{K}^{-1}$ , a 4442% tremendous enhancement compared to the pure patterned TPU fibrous structure ( $0.019 \text{ W m}^{-1}\text{K}^{-1}$ ),

illustrating the formation of the thermally conductive pathways. Furthermore, due to the mechanical robustness of the composite, the thermal conductivity demonstrated outstanding stability. After being bent and stretched (strain  $\sim 100\%$ ) for 800 cycles, the maximum fluctuation of the thermal conductivity of the composite based on 25 wt% BNNs remained within 6.4% and 7.9%, respectively, as shown in Fig. 3f.

### Thermal management capability for flexible electronics

Graphene is now widely used for wearable devices. To validate the thermal management capability of this breathable structure for flexible electronics, further experiments based on graphene were carried out. Firstly, a graphene (Supplementary Fig. 5a) layer was spray-coated on the fibrous patterned grids, then Ecoflex-BNNs layer with different loading of BNNs was deposited onto graphene. In this course, the Ecoflex-BNNs film completely covered graphene can act as electrical insulating packaging layer to prevent graphene from leakage due to the electrical insulation of Ecoflex and BNNs (Supplementary Fig. 5b), and the breathable patterned electrospun fibrous membrane act as thermal insulating layer for wearable electronics. According to the variable loading of graphene, a flexible conductor and/or strain sensor can be fabricated, respectively. After coated graphene, the samples reserved good breathability, and the air permeability was both about  $21.41 \text{ mm s}^{-1}$ , similar to that without graphene.

The flexible conductor with an average electrical resistance of  $800 \Omega$  demonstrated a stable resistance under various bending angle ( $\theta$ ) from  $0^\circ$  (the flat state) to  $140^\circ$  (Supplementary Fig. 6). Under a fixed voltage of 10 V, a small normalized electrical resistance change ( $\Delta R_e/R_{e0}$ ) of 0.103 even under the largest bending angle of  $140^\circ$  (Supplementary Fig. 7) was observed, as well as a good durability under more than 2000 cycles of bending-releasing process between  $0^\circ$  and  $140^\circ$  (Fig. 4a), indicating the well wrapping of graphene by Ecoflex-BNNs. During the operation of the flexible conductor, it was found that the surface temperature of all the samples increased at the beginning, and then reached a saturated state, to the equilibrium operational temperature, within a very short time (Fig. 4b). As expected, the nanocomposites with higher loading of BNNs showed a lower saturating operating temperature. It is worthy to point out that the thermal dissipation in this case is different from that of electronics with a planar surface, because of the curved surface of the samples. From Supplementary Fig. 5b, one can observe that the graphene layer was packaged with the arcuate Ecoflex-BNNs film, thus heat generated from graphene can be dissipated through Ecoflex-BNNs film. In this way, the close-contacted BNNs in the Ecoflex matrix can construct thermally conductive pathways, which ensure rapid thermal transmission. As a result, the equilibrium operational temperature of the sample with 25 wt% BNNs was about  $45.1^\circ\text{C}$ , a 34% dropping than that with pure Ecoflex ( $68.3^\circ\text{C}$ ). During more than 2000 cycles of bending-releasing process between  $0^\circ$  and  $140^\circ$ , the surface temperature fluctuation of the flexible conductor was only within  $0.5^\circ\text{C}$ , as shown in Fig. 4c, demonstrating the superior durability of the sample.

The flexible strain sensor had an average electrical resistance of  $1500 \Omega$  due to the less content of graphene than that of the conductor. Figure 4d showed the curve of  $\Delta R_e/R_{e0}$  in response to the change of the applied bending strain (which can be expressed by the bending angle). It can be seen that the gauge factor (GF)<sup>58</sup> (the slope of resistance versus bending angle) was about 1.0 when the bending angle changed from  $0^\circ$  to  $80^\circ$ . With increasing the curvature, it turn into about 1.80 between the bending angle of  $80^\circ$  and  $140^\circ$  due to the separation of adjacent graphene, showing a linear response to various bending strain (Supplementary Fig. 8), as well as a stable performance during more than 2000 bending-releasing cycles from  $0^\circ$  to  $140^\circ$  (Supplementary Fig. 9). As a result, the strain sensor can be adopted for real-time monitoring of

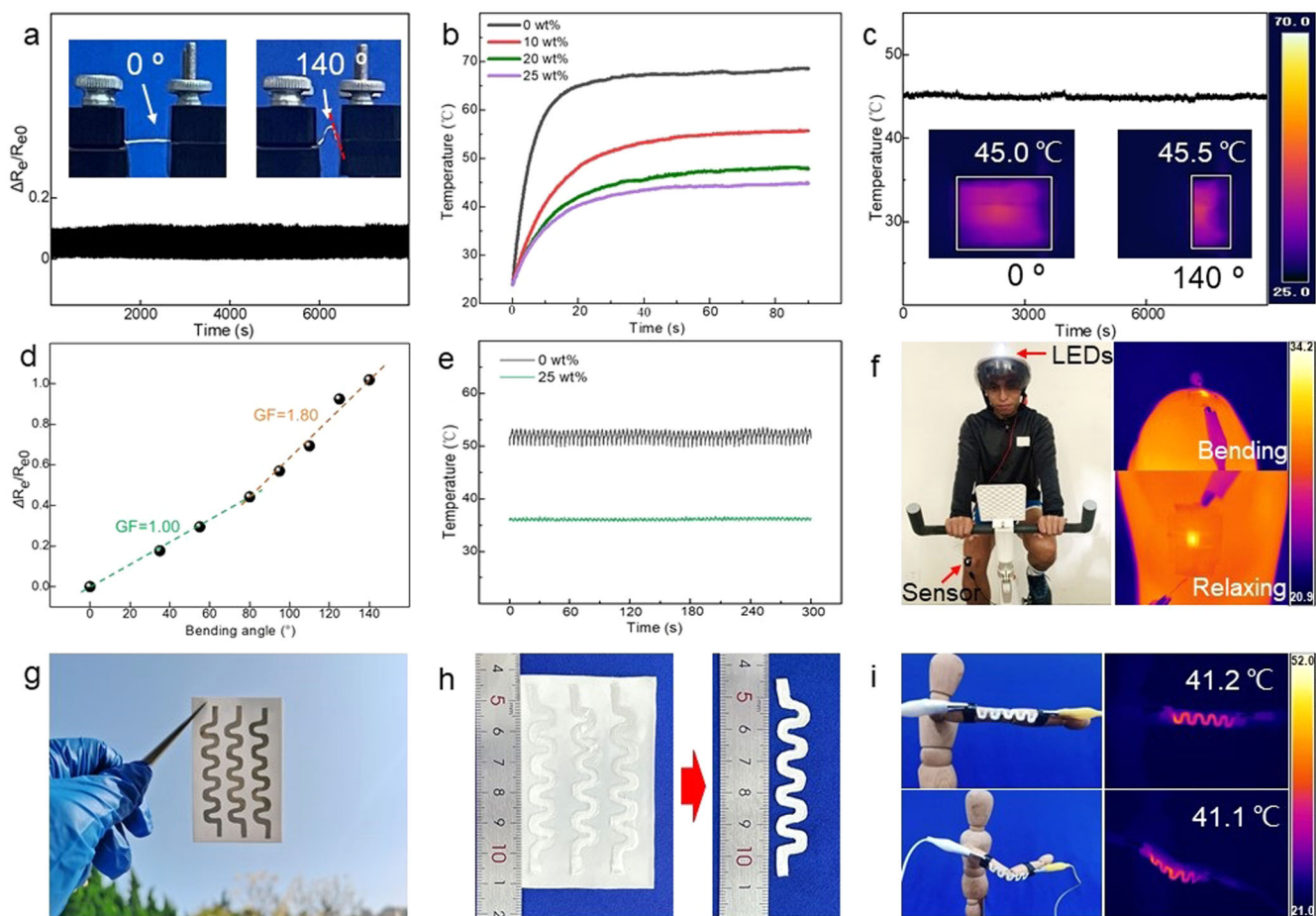


**Fig. 4 Thermal management capability for flexible electronics.** **a** Normalized electrical resistance change ( $\Delta R_e/R_{e0}$ ) of the flexible conductor under more than 2000 cycles of bending-releasing process between  $0^\circ$  and  $140^\circ$ . **b** Comparison of the surface temperature from the beginning to the equilibrium operational temperature within a very short time. **c** During more than 2000 cycles of bending-releasing process between  $0^\circ$  and  $140^\circ$ , the surface temperature fluctuation of the flexible conductor was within  $0.5^\circ\text{C}$ . **d** Curve of  $\Delta R_e/R_{e0}$  in response to the change of the applied bending strain of the flexible strain sensor. **e** Comparison of the equilibrium surface temperature fluctuation of the sample with 25 wt% BNNs and pure Ecoflex during multiple cycles of the bending-releasing process between  $0^\circ$  and  $140^\circ$  of the strain sensor. **f** During the operation of the flexible strain sensor as a warning device for the cyclists, the surface temperature was almost unchanged. Photograph of the printed serpentine flexible electrical conductors onto the Ecoflex-BNNs film (**g**) before and (**h** left) after electrospinning, and (**h** right) is the photograph of single flexible conductor cut along the edge after electrospinning. **i** The surface temperature of the as-cut conductor with 25 wt% BNNs (it was fixed onto the elbow of an IKEA doll. And during elbow flexion and extension).

human motion, such as repeatedly flexion-extension of finger (Supplementary Fig. 10a) and wrist (Supplementary Fig. 10b). During operation of the strain sensor under a 10 V voltage, be the same as that of the conductor, the equilibrium surface temperature of the sensor covered with 25 wt% BNNs had a large decline than that covered pure Ecoflex film, as shown in Supplementary Fig. 11. Interestingly, the designed structure of the composite exhibited a superior thermal management capability. From Fig. 4e, during multiple cycles of the bending-releasing process between  $0^\circ$  and  $140^\circ$  of the strain sensor, the fluctuation of the equilibrium surface temperature of the sample with 25 wt% BNNs was only within  $0.5^\circ\text{C}$ , while the equilibrium surface temperature fluctuation of that with pure Ecoflex was  $3^\circ\text{C}$ , 6 times higher than the former. This reason highlights the construction of thermally conductive pathways in the composite, so that the heat can be dissipated rapidly from the devices.

With the increasing emphasis on human health problems, more and more people engage in regular physical activity. Cycling is one of the most popular forms of exercise not only because of its effects on prevention of chronic diseases such as hypertension<sup>59</sup> and cardiopathy<sup>60</sup>, but also because of its low requirement on space restrictions. However, in some case such as riding at night

with inadequate light, danger may occurred. For example, the driver in a speeding car or truck may not notice the cyclists from a distance due to the lack of effective warning on the cyclists. To this end, we designed a set of warning device by integrating the sensor in a circuit (Supplementary Fig. 12) and a spinning exercise bike was introduced to mimic this situation. Herein, the flexible sensor was attached onto the knee of the cyclist. When the knee is bent and released during cycling, the LEDs on the helmet will flicker (Supplementary Movie 1), and caution can be given to the passing cars or trucks. Interestingly, during the continuously riding process (bending and releasing of the knee), the surface temperature was almost unchanged, as shown in Fig. 4f, which was the same as that during flexing or extending the finger and wrist (Supplementary Fig. 10). It can be ascribed that the excellent thermal dissipation performance of the device help it maintain a low and stable surface temperature.

#### Prototype for wearable electronics with desired architecture and advanced thermal management capability

Patterned electrospun fibrous structure can be assembled according to the morphology of the conductive collector, and it

would be helpful for directly fabricating large-scaled wearable electronics with desired architecture and thermal management capability. Herein, a prototype of this strategy was carried out. Firstly, a flexible thermally conductive Ecoflex-BNNSs film (thickness of  $\sim 0.3$  mm) with 25 wt% BNNSs was fabricated. Followed by a UV/O<sub>3</sub> surface treatment, serpentine flexible electrical conductors (electrical resistance of  $\sim 2 \Omega$ ) based Ag ink were deposited on the film using inkjet printing technology, as shown in Fig. 4g.

We use Ag as an electrical conductive material because of its excellent conductivity and outstanding flexibility, rendering it a suitable candidate for the next-generation wearable devices<sup>61–63</sup>. Particularly, Ag is proved facile and stable for inkjet printing technology, which offers the new opportunity for fabricating wearable electronics with environmentally friendly and cost-effective production process<sup>64,65</sup>.

Because of its good electric conduction of Ag, electrospinning fibers can be deposited on the flexible conductors. After electrospinning for 2 h, it was found that most of the fibers were stored on the conductor with a morphology similar to the conductor (Fig. 4h left). And each serpentine conductor with Ecoflex-BNNSs film and fibers can be cut along the edges in accordance with requirements (Fig. 4h right). Under a voltage of 2.5 V, Joule heat was generated. As a result, the surface temperature of the film packaging side showed obvious difference. The temperature of the sample with 25 wt% BNNSs was much lower than that with pure Ecoflex, as shown in Supplementary Fig. 13, due to the high thermal conductivity of the composite. In addition, the electrospun fibers render a thermal insulating capacity because of the porous structure. One can see that the surface temperature of the fiber packaging sides was lower than that of the film packaging sides, showing the potential that the fibrous sides can be attached closed to human skin to prevent it from burning damage when the devices were operating. When the as-cut conductor with 25 wt% BNNSs was fixed onto the elbow of an IKEA doll, as shown in Fig. 4i, during elbow flexion and extension process, no different surface temperature was observed. This can be understood as the following: after inkjet printing, the Ag film demonstrated a relatively dense structure (Supplementary Fig. 14), which was quite different from that using graphene nanosheets. During the IKEA doll elbow flexion and extension process, it is insufficient to make fracture and/or crack in the Ag flayer, in particular, it is supported by the flexible Ecoflex-BNNSs film. Thus, no obvious resistance change occurs, resulting in a relative stable surface temperature. It indicates the stable thermal management capability and of the sample. All these advantages make it suitable for the fabrication of next-generation of wearable electronics.

## DISCUSSION

In summary, we have provided a simple route to fabricate a composite with both enhanced thermal management capability and remarkable flexibility, while retaining excellent permeability. It has been achieved by depositing Ecoflex-BNNSs layer onto the grids of the patterned electrospun TPU fibrous membrane. Besides a tremendous 4442% enhancement of the thermal conductivity compared to that of the pure patterned fibrous structure, the breathability had a minimal degradation. When applied for the wearable electronics, the saturating operating temperature of the sample demonstrated a drastic dropping compared to that with pure Ecoflex packaging. And even under more than 2000 cycles of continuously bending-releasing process, the surface temperature fluctuation was within 0.5 °C, indicating the thermal stability of the composite. Finally, due to the merits of electrospinning, a prototype to prepare wearable electronics with desired architecture and advanced thermal management capability has been

presented. We believe that our results provide an insight in fabrication of next-generation of wearable devices.

## METHODS

### Exfoliation of h-BN

Liquid phase exfoliation of BNNSs from hexagonal boron nitride (h-BN) was carried out according to our previous work<sup>1,40,41</sup>. Firstly, 3.5 g of h-BN powders was added into a 200 mL mixture solvent of isopropanol and deionized water (1:1 by weight). After sonicating the solution in a sonication bath for 4 h with a frequency of 20 kHz, the dispersions were centrifuged at 4000 rpm for 10 min to remove the non-exfoliated h-BN. Finally, the supernatants were collected and centrifuged at 9000 rpm for 30 min, and BNNSs were obtained.

### Electrospun patterned TPU fibrous membrane

First, dimethylformamide (DMF) and tetrahydrofuran (THF) were mixed 1:1 by weight as solvent. The TPU particles were continuously stirred in a solvent with a concentration of 15 wt% for 3 h until a uniform electrospinning precursor solution was formed. For electrospinning, an electrospinning machine supplied by Qingdao Nokang Environmental Protection Technology Co., Ltd was adopted, and the steel wire mesh was used as collector to obtain patterned TPU fibrous membrane. During electrospinning, the applied voltage was about 15 kV, and the working distance between the spinneret and the collector was about 16 cm. The electrospinning time was 8 h. All electrospinning experiments were carried out at room temperature and ambient humidity of 20–50% RH.

### Fabrication of high thermally conductive composites

Firstly, solution of Ecoflex-BN was prepared. Ecoflex rubbers are mixed 1A:1B by weight. Then BNNSs was added to 1 g of A and stirred for 30 min. Finally, 1 g B was added and continue stirring until the solution was uniform. Thus, Ecoflex-BNNSs solution with different contents of BNNSs was obtained. For comparison, the contents of BNNSs was chosen as 10 wt%, 20 wt%, and 25 wt%, respectively. The as-prepared Ecoflex-BNNSs solution was coated onto the grids of the patterned TPU fibrous membrane with the aid of a metal mask.

To fabricate the wearable conductor and strain sensor, graphene was firstly spray-coated onto patterned TPU fibrous membrane to form specific conductive pathways using the metal mask. Then the Ecoflex-BNNSs solution was coated onto the graphene surface through the mask. After vacuum drying for 6 h, two Cu foils were attached on both naked ends of the fibrous membrane, and the devices were fabricated.

The serpentine flexible electrical conductor arrays was fabricated by a pneumatic extrusion type flexible electronics printer (MP1100, Prtronic, Shanghai, China), and the commercial Ag ink (BASE-CD01) was used. After inkjet printing for about 45 min, the samples were suffered from a vacuum drying at 120 °C for half one hour to remove the solvent.

### Characterization

The morphology and the microstructure of the samples were characterized by a field-emission SEM (Nova Nano SEM 450, FEI, USA). The optical photographs of the samples were captures by a Huawei mobile phone (Huawei P 40). The electrical properties were obtained using Keithley 6485 high-resistance meter system, and the strain-stress curves of the samples were measured by a dynamical mechanical analyzer (Q-800, TA Scientific). Thermal conductivity ( $k$ ) of the samples was tested using Hot Disk TPS 2500S. The permeability of the samples was measured by a digital air permeability measuring instrument (YG461E-11). Surface

temperature was captured via an infrared thermograph (FOTRIC-226-2, China).

## DATA AVAILABILITY

The data that support the findings of this study are available from the corresponding author on request.

Received: 6 January 2023; Accepted: 23 April 2023;

Published online: 08 May 2023

## REFERENCES

1. Tan, C. et al. A high performance wearable strain sensor with advanced thermal management for motion monitoring. *Nat. Commun.* **11**, 3530 (2020).
2. Stadlober, B., Zirkl, M. & Irimia-Vladu, M. Route towards sustainable smart sensors: ferroelectric polyvinylidene fluoride-based materials and their integration in flexible electronics. *Chem. Soc. Rev.* **48**, 1787–1825 (2019).
3. Chung, H. U. et al. Binodal, wireless epidermal electronic systems with in-sensor analytics for neonatal intensive care. *Science* **363**, eaau0780 (2019).
4. Wang, Y. et al. A durable nanomesh on-skin strain gauge for natural skin motion monitoring with minimum mechanical constraints. *Sci. Adv.* **6**, eabb7043 (2020).
5. Yin, L. et al. A stretchable epidermal sweat sensing platform with an integrated printed battery and electrochromic display. *Nat. Electron.* **5**, 694–705 (2022).
6. Song, J., Lee, H., Jeong, E. G., Choi, K. C. & Yoo, S. Organic light-emitting diodes: pushing toward the limits and beyond. *Adv. Mater.* **32**, 1907539 (2020).
7. Matsuhsu, N. et al. High-frequency and intrinsically stretchable polymer diodes. *Nature* **600**, 246–252 (2021).
8. Kim, J.-H. & Park, J.-W. Intrinsically stretchable organic light-emitting diodes. *Sci. Adv.* **7**, eabd9715 (2021).
9. Strassburg, S., Zainuddin, S. & Scheibel, T. The power of silk technology for energy applications. *Adv. Energy Mater.* **11**, 2100519 (2021).
10. Lai, Y. C. et al. Elastic multifunctional liquid-metal fibers for harvesting mechanical and electromagnetic energy and as self-powered sensors. *Adv. Energy Mater.* **11**, 2100411 (2021).
11. Vallem, V., Sargolzaeiaval, Y., Ozturk, M., Lai, Y. C. & Dickey, M. D. Energy harvesting and storage with soft and stretchable materials. *Adv. Mater.* **33**, 2004832 (2021).
12. Jian, G. et al. Excellent high-temperature piezoelectric energy harvesting properties in flexible polyimide/3D PbTiO<sub>3</sub> flower composites. *Nano Energy* **82**, 105778 (2021).
13. Zohair, M. et al. Continuous energy harvesting and motion sensing from flexible electrochemical nanogenerators: toward smart and multifunctional textiles. *ACS Nano* **14**, 2308–2315 (2020).
14. Dai, M. et al. Robust piezo-phototronic effect in multilayer  $\gamma$ -InSe for high-performance self-powered flexible photodetectors. *ACS Nano* **13**, 7291–7299 (2019).
15. Cai, S., Xu, X., Yang, W., Chen, J. & Fang, X. Materials and designs for wearable photodetectors. *Adv. Mater.* **31**, 1808138 (2019).
16. Huang, Z. et al. Three-dimensional integrated stretchable electronics. *Nat. Electron.* **1**, 473–480 (2018).
17. Yang, Q. et al. Photocurable bioresorbable adhesives as functional interfaces between flexible bioelectronic devices and soft biological tissues. *Nat. Mater.* **20**, 1559–1570 (2021).
18. Yin, R., Wang, D., Zhao, S., Lou, Z. & Shen, G. Wearable sensors-enabled human-machine interaction systems: from design to application. *Adv. Funct. Mater.* **31**, 2008936 (2020).
19. Dai, Z. et al. One-step preparation of a core-spun Cu/P(VDF-TrFE) nanofibrous yarn for wearable smart textile to monitor human movement. *ACS Appl. Mater. Interfaces* **13**, 44234–44242 (2021).
20. Yin, J., Hinchet, R., Shea, H. & Majidi, C. Wearable soft technologies for haptic sensing and feedback. *Adv. Funct. Mater.* **31**, 2007428 (2020).
21. Qi, D., Liu, Z., Leow, W. R. & Chen, X. Elastic substrates for stretchable devices. *MRS Bull.* **42**, 103–107 (2017).
22. Sun, B. & Huang, X. Seeking advanced thermal management for stretchable electronics. *npj Flex. Electron.* **5**, 12 (2021).
23. Ma, Z. et al. Permeable superelastic liquid-metal fibre mat enables biocompatible and monolithic stretchable electronics. *Nat. Mater.* **20**, 859–868 (2021).
24. Miyamoto, A. et al. Inflammation-free, gas-permeable, lightweight, stretchable on-skin electronics with nanomeshes. *Nat. Nanotechnol.* **12**, 907–913 (2017).
25. Liu, Z. et al. Highly breathable and stretchable strain sensors with insensitive response to pressure and bending. *Adv. Funct. Mater.* **31**, 2007622 (2021).
26. Gao, Q. et al. Breathable and flexible polymer membranes with mechano-responsive electric resistance. *Adv. Funct. Mater.* **30**, 1907555 (2020).
27. Wang, X., Liu, X. & Schubert, D. W. Highly sensitive ultrathin flexible thermoplastic polyurethane/carbon black fibrous film strain sensor with adjustable scaffold networks. *Nano Micro Lett.* **13**, 64 (2021).
28. Chen, J., Huang, X., Sun, B. & Jiang, P. Highly thermally conductive yet electrically insulating polymer/boron nitride nanosheets nanocomposite films for improved thermal management capability. *ACS Nano* **13**, 337–345 (2019).
29. Guo, Y., Qiu, H., Ruan, K., Zhang, Y. & Gu, J. Hierarchically multifunctional polyimide composite films with strongly enhanced thermal conductivity. *Nano Micro Lett.* **14**, 26 (2021).
30. Zhang, F. et al. Stress controllability in thermal and electrical conductivity of 3D elastic graphene-crosslinked carbon nanotube sponge/polyimide nanocomposite. *Adv. Funct. Mater.* **29**, 1901383 (2019).
31. Cai, Q. et al. High thermal conductivity of high-quality monolayer boron nitride and its thermal expansion. *Sci. Adv.* **5**, eaav0129 (2019).
32. Hong, H. et al. Anisotropic thermal conductive composite by the guided assembly of boron nitride nanosheets for flexible and stretchable electronics. *Adv. Funct. Mater.* **29**, 1902575 (2019).
33. van Erp, R., Soleimanzadeh, R., Nela, L., Kampitsis, G. & Matioli, E. Co-designing electronics with microfluidics for more sustainable cooling. *Nature* **585**, 211–216 (2020).
34. Chen, H. et al. Thermal conductivity of polymer-based composites: fundamentals and applications. *Prog. Polym. Sci.* **59**, 41–85 (2016).
35. Burger, N. et al. Review of thermal conductivity in composites: mechanisms, parameters and theory. *Prog. Polym. Sci.* **61**, 1–28 (2016).
36. Zeller, R. C. & Pohl, R. O. Thermal conductivity and specific heat of noncrystalline solids. *Phys. Rev. B* **4**, 2029–2041 (1971).
37. Li, T. et al. Stretchable phosphor/boron nitride nanosheet/polydimethylsiloxane films for thermal management and rapid monitoring. *ACS Appl. Polym. Mater.* **4**, 1431–1439 (2022).
38. Sun, B. et al. Electrospun anisotropic architectures and porous structures for tissue engineering. *J. Mater. Chem. B* **3**, 5389–5410 (2015).
39. Zhao, S., Zhou, Q., Long, Y. Z., Sun, G. H. & Zhang, Y. Nanofibrous patterns by direct electrospinning of nanofibers onto topographically structured non-conductive substrates. *Nanoscale* **5**, 4993–5000 (2013).
40. Chen, J. et al. Vertically aligned and interconnected boron nitride nanosheets for advanced flexible nanocomposite thermal interface materials. *ACS Appl. Mater. Interfaces* **9**, 30909–30917 (2017).
41. Wang, Q. et al. AWI-assembled TPU-BNNS composite films with high in-plane thermal conductivity for thermal management of flexible electronics. *ACS Appl. Mater. Interfaces* **14**, 41447–41455 (2022).
42. Bhanushali, S., Ghosh, P. C., Simon, G. P. & Cheng, W. Copper nanowire-filled soft elastomer composites for applications as thermal interface materials. *Adv. Mater. Interfaces* **4**, 1700387 (2017).
43. Liu, X. et al. Recent progress on smart fiber and textile based wearable strain sensors: materials, fabrications and applications. *Adv. Fiber Mater.* **4**, 361–389 (2022).
44. Liu, Z. et al. Functionalized fiber-based strain sensors: pathway to next-generation wearable electronics. *Nano Micro Lett.* **14**, 61 (2022).
45. Ma, J. et al. Thermal conductivity of electrospun polyethylene nanofibers. *Nanoscale* **7**, 16899–16908 (2015).
46. Zhang, Y. et al. Thermal transport in electrospun vinyl polymer nanofibers: effects of molecular weight and side groups. *Soft Matter* **14**, 9534–9541 (2018).
47. Zhong, Z. et al. Structure-induced enhancement of thermal conductivities in electrospun polymer nanofibers. *Nanoscale* **6**, 8283–8291 (2014).
48. Bartlett, M. D. et al. High thermal conductivity in soft elastomers with elongated liquid metal inclusions. *Proc. Natl Acad. Sci. USA* **114**, 2143–2148 (2017).
49. Shen, S., Henry, A., Tong, J., Zheng, R. & Chen, G. Polyethylene nanofibres with very high thermal conductivities. *Nat. Nanotechnol.* **5**, 251–255 (2010).
50. Cui, Y., Qin, Z., Wu, H., Li, M. & Hu, Y. Flexible thermal interface based on self-assembled boron arsenide for high-performance thermal management. *Nat. Commun.* **12**, 1284 (2021).
51. Shi, L. et al. Measuring thermal and thermoelectric properties of one-dimensional nanostructures using a microfabricated device. *J. Heat. Transf.* **125**, 881–888 (2003).
52. Xu, X. et al. Length-dependent thermal conductivity in suspended single-layer graphene. *Nat. Commun.* **5**, 3689 (2014).
53. Dong, L. et al. Dimensional crossover of heat conduction in amorphous polyimide nanofibers. *Natl Sci. Rev.* **5**, 500–506 (2018).
54. Yu, C. et al. Thermal contact resistance and thermal conductivity of a carbon nanofiber. *J. Heat. Transf.* **128**, 234–239 (2006).
55. Bi, K. et al. Lodine doping effects on the lattice thermal conductivity of oxidized polyacetylene nanofibers. *J. Appl. Phys.* **114**, 194302 (2013).
56. Aiyiti, A., Bai, X., Wu, J., Xu, X. & Li, B. Measuring the thermal conductivity and interfacial thermal resistance of suspended MoS<sub>2</sub> using electron beam self-heating technique. *Sci. Bull.* **63**, 452–458 (2018).



57. Liu, B., Chen, Y. & Xu, X. Thermal manipulation and thermal rectification in pi-stacked organic nanowires. *Nanoscale* **13**, 13641–13649 (2021).
58. Kim, S. J. et al. High durability and waterproofing rGO/SWCNT-fabric-based multifunctional sensors for human-motion detection. *ACS Appl. Mater. Interfaces* **10**, 3921–3928 (2018).
59. Valli, G. et al. Pathophysiological adaptations to walking and cycling in primary pulmonary hypertension. *Eur. J. Appl. Physiol.* **102**, 417–424 (2008).
60. Gurzäu, D. et al. The role of cardiovascular rehabilitation in women with ischemic heart disease and rhythm disorders. *Balneo Res. J.* **9**, 50–53 (2018).
61. Choi, S. et al. Highly conductive, stretchable and biocompatible Ag-Au core-sheath nanowire composite for wearable and implantable bioelectronics. *Nat. Nanotechnol.* **13**, 1048–1056 (2018).
62. Xie, Z. et al. Flexible and stretchable antennas for biointegrated electronics. *Adv. Mater.* **32**, 1902767 (2020).
63. Yang, Y., Duan, S. & Zhao, H. Advances in constructing silver nanowire-based conductive pathways for flexible and stretchable electronics. *Nanoscale* **14**, 11484–11511 (2022).
64. Park, J. et al. Highly customizable all solution-processed polymer light emitting diodes with inkjet printed Ag and transfer printed conductive polymer electrodes. *Adv. Funct. Mater.* **29**, 1902412 (2019).
65. Liu, Y. et al. Recent advances of inkjet-printing technologies for flexible/wearable electronics. *Nanoscale* **15**, 6025–6051 (2023).

## ACKNOWLEDGEMENTS

This study was supported by the Natural Science Foundation of Shandong Province (ZR2020ME193), the National Natural Science Foundation of China (62004211), and Shenzhen Science and Technology Program (RCBS20200714114858221). We thank Dr. Xiyue Cao (Instrumental Analysis Center, Qingdao University) for the help of SEM testing.

## AUTHOR CONTRIBUTIONS

B.S. supervised the project and wrote the paper. B.S., G.Z., Y.Z. and X.B. designed the project, discussed the results and write the manuscript. B.L. and T.-Y.Z. supervised the project, discuss the results and revised the manuscript. H.C. and Y.D. carried out the experiments and analyzed the data. Y.L. and X.L. conducted the SEM characterizations. Y.L. fabricated the flexible conductor using inkjet printing. Q.F. contributed to

the test of flexible sensor. Y.Z. contributed to the permeability of the sample. X.H. tested the thermal conductivity.

## COMPETING INTERESTS

The authors declare no competing interests.

## ADDITIONAL INFORMATION

**Supplementary information** The online version contains supplementary material available at <https://doi.org/10.1038/s41528-023-00257-0>.

**Correspondence** and requests for materials should be addressed to Guimei Zhu, Xue Bai, Yan Zhao or Bin Sun.

**Reprints and permission information** is available at <http://www.nature.com/reprints>

**Publisher's note** Springer Nature remains neutral with regard to jurisdictional claims in published maps and institutional affiliations.



**Open Access** This article is licensed under a Creative Commons Attribution 4.0 International License, which permits use, sharing, adaptation, distribution and reproduction in any medium or format, as long as you give appropriate credit to the original author(s) and the source, provide a link to the Creative Commons license, and indicate if changes were made. The images or other third party material in this article are included in the article's Creative Commons license, unless indicated otherwise in a credit line to the material. If material is not included in the article's Creative Commons license and your intended use is not permitted by statutory regulation or exceeds the permitted use, you will need to obtain permission directly from the copyright holder. To view a copy of this license, visit <http://creativecommons.org/licenses/by/4.0/>.

© The Author(s) 2023